© 2018. Published by The Company of Biologists Ltd | Journal of Cell Science (2018) 131, jcs212092. doi:10.1242/jcs.212092

RESEARCH ARTICLE

Ki-67 and condensins support the integrity of mitotic chromosomes through distinct mechanisms

Masatoshi Takagi[1,*], Takao Ono[2], Toyoaki Natsume[3], Chiyomi Sakamoto[4], Mitsuyoshi Nakao[4], Noriko Saitoh[4,5], Masato T. Kanemaki[3], Tatsuya Hirano[2] and Naoko Imamoto[1]

ABSTRACT

Although condensins play essential roles in mitotic chromosome assembly, Ki-67 (also known as MKI67), a protein localizing to the periphery of mitotic chromosomes, had also been shown to make a contribution to the process. To examine their respective roles, we generated a set of HCT116-based cell lines expressing Ki-67 and/or condensin subunits that were fused with an auxin-inducible degron for their conditional degradation. Both the localization and the dynamic behavior of Ki-67 on mitotic chromosomes were not largely affected upon depletion of condensin subunits, and vice versa. When both Ki-67 and SMC2 (a core subunit of condensins) were depleted, ball-like chromosome clusters with no sign of discernible thread-like structures were observed. This severe defective phenotype was distinct from that observed in cells depleted of either Ki-67 or SMC2 alone. Our results show that Ki-67 and condensins, which localize to the external surface and the central axis of mitotic chromosomes, respectively, have independent yet cooperative functions in supporting the structural integrity of mitotic chromosomes.

KEY WORDS: Ki-67, Condensin, Mitotic chromosome, Auxin-inducible degron, AID

INTRODUCTION

During the mitosis of animal cells, the nuclear envelope breaks down and chromatin surrounded by the nuclear envelope is packaged into a discrete set of rod-shaped structures, known as mitotic chromosomes. This process enables different chromosomes to untangle, duplicated chromatids to resolve and sister kinetochores to properly attach to the mitotic spindle, thereby ensuring the faithful segregation of genetic materials into daughter cells. Extensive studies during the past two decades have established that a class of multiprotein complexes, condensins, play central roles in mitotic chromosome assembly and segregation (Hirano, 2016; Uhlmann, 2016). Most eukaryote species have two different types of condensin complexes (condensins I and II). The two complexes share the same pair of structural maintenance of chromosome (SMC) ATPase subunits (SMC2 and SMC4), and have distinct sets of non-SMC regulatory proteins [CAP-H, -D2 and -G for condensin I (also known as NCAPH, NCAPD2 and NCAPG, respectively), and CAP-H2, -D3 and -G2 for condensin II (also known as NCAPH2, NCAPD3 and NCAPG2, respectively)]. A recent study has shown that structures reminiscent of mitotic chromosomes can be reconstituted *in vitro* using a limited number of purified factors, including core histones, three histone chaperones, topoisomerase IIα (topo IIα) and condensin I (Shintomi et al., 2015). It is clear, however, that this list represents a minimum set of proteins required for building mitotic chromosomes, and that additional proteins must cooperate to provide them with physical and physicochemical properties that support and promote their own segregation. Candidates for such proteins include linker histones (Maresca et al., 2005), the chromokinesin KIF4 (Mazumdar et al., 2006; Samejima et al., 2012; Takahashi et al., 2016) and Ki-67 (also known as MKI67) (Booth et al., 2016; Takagi et al., 2016).

Ki-67 is a nucleolar protein widely appreciated as a cell proliferation marker (Scholzen and Gerdes, 2000). During mitosis, Ki-67 is localized around mitotic chromosomes and constitutes a perichromosomal layer to which many nucleolar proteins are targeted (Booth et al., 2014; Takagi et al., 2014). To assess the mitotic function of Ki-67, we have recently generated HCT116-based cell lines in which endogenous Ki-67 can be degraded conditionally and acutely via an auxin-inducible degron (AID) (Takagi et al., 2016). By using these cell lines, we have demonstrated that Ki-67 aids the completion of mitotic chromosome assembly and the maintenance of rod-shaped chromosome structures (Takagi et al., 2016). Another recent study has demonstrated that Ki-67 may act as a biological 'surfactant' to prevent the coalescence of mitotic chromosomes by using its positively charged, extended conformation that orients perpendicular to the surface of mitotic chromosomes (Cuylen et al., 2016). Despite these intriguing observations, it remains unclear how the perichromosomally localized proteins, such as Ki-67, might functionally cooperate with the axially localized proteins, such as condensins, to build individual chromosomes and to support their segregation during mitosis.

In the current study, we aimed to address this question by conditionally depleting Ki-67 and condensin subunits individually or simultaneously from mitotic cells. To this end, we generated a panel of HCT116-based cell lines expressing Ki-67 and/or condensin subunits that were fused with an AID for their conditional degradation and with fluorescent proteins for imaging. Remarkably, ball-like chromosome clusters with no sign of discernible thread-like structures were observed in mitotic cells depleted of both Ki-67 and SMC2. To further assess this unprecedented 'rice cake' phenotype, we performed a quantitative analysis with a supervised machine-learning algorithm, wndchrm (Ono et al., 2017; Orlov et al., 2008). We also present evidence that aberrant kinetochore–microtubule attachments accompany the formation of the rice cake. The observations presented here argue that Ki-67 and condensins, which localize to the external surface and the central axis of mitotic chromosomes, respectively, have independent yet cooperative functions in supporting the structural integrity of mitotic chromosomes in mammalian cells.

[1]Cellular Dynamics Laboratory, RIKEN, Wako 351-0198, Japan. [2]Chromosome Dynamics Laboratory, RIKEN, Wako 351-0198, Japan. [3]Division of Molecular Cell Engineering, NIG, Mishima 411-8540, Japan. [4]Department of Medical Cell Biology, IMEG, Kumamoto University, Kumamoto 860-0811, Japan. [5]Department of Cancer Biology, The Cancer Institute of JFCR, Tokyo 135-8550, Japan.

*Author for correspondence (mtakagi@riken.jp)

M.T., 0000-0002-7580-9184

Received 12 October 2017; Accepted 15 February 2018

Journal of Cell Science (2018) 131, jcs212092. doi:10.1242/jcs.212092

RESULTS

Ki-67, CAP-H and CAP-H2 localize on mitotic chromosomes independently from one another

We previously generated an HCT116-based cell line (AID2) in which endogenous Ki-67 is fused to mAID and mClover (mACl), thereby enabling us to degrade Ki-67 conditionally upon addition of indol-3-acetic acid (IAA) (Takagi et al., 2016). To examine the localization of CAP-H (a subunit specific to condensin I) and CAP-H2 (a subunit specific to condensin II) in the absence of Ki-67, we further modified AID2 [herein renamed Ki-67-mACl (#2)] by a CRISPR-mediated knock-in strategy, to generate Ki-67-mACl/CAP-H-Ch (#11) and Ki-67-mACl/CAP-H2-Ch (#44), in which CAP-H and CAP-H2, respectively, were C-terminally fused to mCherry. Ki-67-mACl/CAP-H-Ch (#11) and Ki-67-mACl/CAP-H2-Ch (#44) cells were synchronized to the G2 phase by inhibiting Cdk1 with RO-3306 in the presence or absence of IAA, and then released into M phase in the presence of S-trityl-L-cysteine (STLC), a KIF11 (also known as Eg5) inhibitor (Fig. 1A). At 1 h after the release, the cells were subjected to immunoblot analysis (Fig. 1B) and microscopy observation (Fig. 1C,D). In both cell lines, Ki-67 fused to mACl was degraded upon addition of IAA (Fig. 1B, lanes 3 and 6) as had been shown in their ancestor cell line Ki-67-mACl (#2) (Takagi et al., 2016). Whereas CAP-H–mCherry and CAP-H2–mCherry were detected at positions ∼25 kDa bigger than their endogenous counterparts in the blots due to the mCherry tagging (at positions of ∼125 and 110 kDa, respectively), no signal was detected at the size of their endogenous counterparts (lanes 2–3 and 5–6), indicating that both alleles of their genomes had been edited as intended. In a subpopulation of IAA-treated cells (∼10% at most), the fluorescence signal of Ki-67–mACl was still detectable in this experimental condition. In the microscopy observation, we focused on cells in which the signal decreased to an undetectable level. We found that both CAP-H–mCherry and CAP-H2–mCherry localized at the axial regions of mitotic chromosomes, similar to what is seen for the endogenous counterparts even though the overall morphology of chromosomes slightly swelled upon Ki-67 degradation (Fig. 1C,D), a result consistent with the previous observation obtained by immunofluorescence studies using specific antibodies (Takagi et al., 2016).

We then wished to investigate the localization of Ki-67 in the absence of CAP-H or CAP-H2. To this end, we generated CAP-H-mACh (#12) and CAP-H2-mACh (#13) in which CAP-H and CAP-H2, respectively, were C-terminally fused to mAID and mCherry (mACh). Their conditional degradation upon addition of IAA was verified by immunoblot analysis (Fig. 1E; Fig. S1A,B) and microscopy observation (Fig. 1F,G). Upon depletion of either CAP-H or CAP-H2, the perichromosomal localization of Ki-67 was not significantly altered (Fig. 1F,G). Taken together, we conclude that Ki-67 and CAP-H and -H2 localize on mitotic chromosomes independently of one another.

Ki-67 displays its perichromosomal localization and associates dynamically with mitotic chromosomes regardless of the presence or absence of SMC2

To determine unequivocally whether Ki-67 localizes to the periphery of mitotic chromosomes independently of condensins, we wished to generate a cell line in which SMC2, an ATPase subunit that is present in both condensins I and II, was C-terminally fused to mACh. We first attempted to generate such a cell line based on the standard protocol using NIG272 as a mother cell line, in which *Oryza sativa* (*Os*)TIR1, a ubiquitin E3 enzyme specific to AID-tagged proteins, was expressed constitutively, but this was without success, possibly due to reduced expression of SMC2 in the absence of IAA (discussed in Natsume et al., 2016). We circumvented this problem by using NIG430 as a mother cell line, in which *Os*TIR1 was expressed conditionally upon addition of doxycycline (DOX) (Natsume et al., 2016). The resultant cell line, SMC2-mACh (#30), was treated according to the protocol shown in Fig. 2A, and then subjected to immunoblot analysis (Fig. 2B; Fig. S1F) and microscopy observation (Fig. 2C,D). We noticed that degradation of SMC2–mACh upon the treatment with IAA was inefficient in SMC2–mACh (#30) cells, probably because of a lower expression level of *Os*TIR1 compared to that seen in the mother cell line (NIG430) (Fig. 2B). Reflecting this, variable levels of the SMC2–mACh signal were detected among individual cells treated with IAA (Fig. 2C,D). Cells where SMC2–mACh was reduced to less than 25% of the original level upon the treatment with IAA were rare (15 out of 127 cells, 11.8%; Fig. 2C). We noticed, however, that, in all cells with undetectable levels of SMC2–mACh, chromosomes lost their slim rod-like shapes (Fig. 2D, the third row) and contracted into a smaller space (Fig. 2D,E). A similar observation was made also by live-cell imaging (Fig. S2A–C). Although it became hard to distinguish the shape of each chromosome in these cells, it was still possible to trace Ki-67 on the poorly organized chromosomes (Fig. 2D), indicating that SMC2 is largely dispensable for the perichromosomal localization of Ki-67.

We then wished to test whether depletion of SMC2 might affect this dynamic behavior of Ki-67 by performing fluorescence recovery after photobleaching (FRAP) experiments (Saiwaki et al., 2005). According to the protocol depicted in Fig. S3A, Ki-67-mACl/CAP-H-mACh (#14) (characterized in Fig. S4) were transfected twice with control siRNA (siControl) or siRNA against SMC2 (siSMC2), treated with reagents for synchronization, and then subjected to FRAP experiments. We measured the FRAP of Ki-67–mACl in cells with undetectable levels of CAP-H–mACh (Fig. S3D,E), and found that it was indistinguishable from that observed in the control cells (Fig. S3B,C). These results indicate that the dynamic behavior of Ki-67 on the periphery of chromosomes does not depend on SMC2 or the chromatin structure supported by condensins.

Chromosomes rapidly lose their structural integrity upon nuclear envelope breakdown in cells devoid of both Ki-67 and SMC2

In the absence of either Ki-67 (Fig. 1C,D) or SMC2 (Fig. 2D), the architecture of mitotic chromosomes was compromised in different manners, suggesting that Ki-67 and condensins contribute to this event through distinct molecular mechanisms. To further examine the functional relationship between Ki-67 and condensins, we sought to deplete these chromosomal components simultaneously. To this end, we generated another cell line Ki-67-mACl/SMC2-mACh (#35), in which Ki-67 and SMC2 were C-terminally tagged with mACl and mACh, respectively. Ki-67-mACl/SMC2-mACh (#35) cells were treated according to the protocol shown in Fig. 3A. Cell lysates were prepared and subjected to immunoblot analysis to confirm that the bulk levels of the target proteins were reduced in the presence of IAA (Fig. 3B; Fig. S1E). Microscopy inspection of individual cells revealed that the Ki-67–mACl levels were reduced to less than 20% of the original level in 59% of IAA-treated cells (19 out of 32 cells) inspected (Fig. 3C). Live-cell imaging of Ki-67-mACl/SMC2-mACh (#35) cells demonstrated that, in the absence of IAA, the behaviors of Ki-67-mACl and SMC2-mACh were indistinguishable from those of their endogenous counterparts (Fig. 3D). We then monitored cells in which the signals of Ki-67 and SMC2 effectively disappeared in the presence of IAA (Fig. 3E). We found that chromosome compaction

Journal of Cell Science (2018) 131, jcs212092. doi:10.1242/jcs.212092

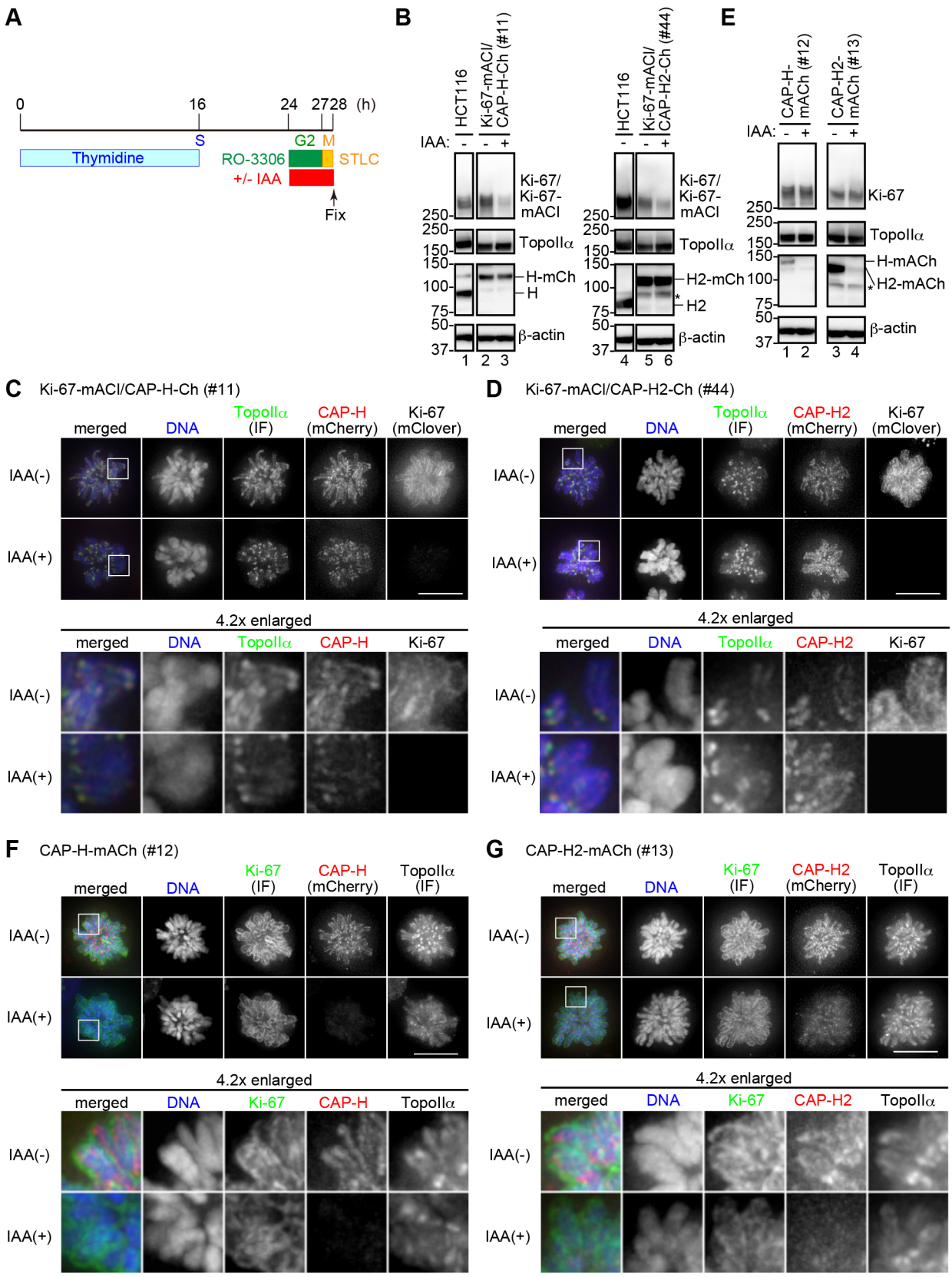

Fig. 1. See next page for legend.

in the prophase nucleus was compromised in these cells [Fig. 3E, time −10 min from nuclear envelope breakdown (NEBD)], as expected from the previous studies reporting condensin depletion (Ono et al., 2004; Hirota et al., 2004), but not in cells devoid of Ki-67 alone (Fig. S5; Takagi et al., 2016). When Ki-67-mAcI/SMC2-mAcH (#35) cells treated with IAA entered prometaphase, a

Journal of Cell Science

Journal of Cell Science (2018) 131, jcs212092. doi:10.1242/jcs.212092

Fig. 1. Ki-67 and CAP-H and -H2 localize on mitotic chromosomes independently from one another. (A) Schematic diagram of the cell preparation protocol. Thymidine (2 mM), RO-3306 (10 µM), STLC (10 µM), and IAA (0.5 mM) were added and/or washed out at the indicated time points. AID-tagged proteins are subjected to proteasome-mediated degradation upon the treatment of cells with IAA for 4 h. (B) Immunoblot analysis of HCT116 (control), Ki-67-mACl/ CAP-H-Ch (#11) and Ki-67-mACl/CAP-H2-Ch (#44) cells. Membranes were probed with specific antibodies against the indicated proteins. The asterisk indicates a non-specific band. (C,D) Immunofluorescence analysis of Ki-67-mACl/ CAP-H-Ch (#11) and Ki-67-mACl/CAP-H2-Ch (#44) cells prepared in the absence (–) or presence (+) of IAA. Ki-67 and CAP-H/H2 were detected via the fluorescence of mClover and mCherry, respectively, fused to their C-terminal ends. Topo IIα was detected by indirect immunofluorescence (IF) using a specific antibody. DNA was counterstained with Hoechst 33342. (E) Immunoblot analysis of CAP-H-mACh (#12) and CAP-H2-mACh (#13) cells. Membranes were probed with specific antibodies against the indicated proteins. The asterisk indicates a non-specific band. (F,G) Immunofluorescence analysis of CAP-H-mACh (#12) and CAP-H2-mACh (#13) cells prepared in the absence (–) or presence (+) of IAA. CAP-H and CAP-H2 were detected via the fluorescence of mCherry fused to their C-terminal ends. Ki-67 and topo IIα were detected by indirect immunofluorescence (IF) using specific antibodies. DNA was counterstained with Hoechst 33342. The areas indicated by the white squares are 4.2-times enlarged and shown on the bottom. Scale bars: 10 µm.

striking phenotype in chromosome morphology was observed coincident with nuclear envelope breakdown (NEBD). At 10 min after NEBD and thereafter, chromatin formed a single cluster, displaying a ball-like structure in which the shape and border of individual chromosomes were not discerned (Fig. 3E, time 10–40 min). To our knowledge, this type of abnormal chromosome structures in mitotic cells had not been reported in the literature before: we therefore refer to this unprecedented structure as a 'rice cake' (rice cake is a Japanese traditional cuisine which is sticky and elastic). Interestingly, the rice cake was frequently observed at one side of the cytoplasm, being placed at the vicinity of the cell cortex. Moreover, part of the rice cake seemed to be pulled in the opposite direction, forming 'protrusions' that were readily discernible with Hoechst 33342 staining.

Mitotic chromosomes rapidly lose their structural integrity upon the degradation of both Ki-67 and SMC2 even after their assembly is complete

We next wished to test what would happen when the degradation of both Ki-67 and SMC2 was induced after mitotic chromosome assembly was complete. To this end, we treated Ki-67-mACl/ SMC2-mACh (#35) cells with the protocol depicted in Fig. 4A. In this protocol, IAA was added 1 h after removing RO-3306 (rather than being added at the same time of RO-3306 addition). At the time point when IAA was added, the cell had already entered mitosis, displaying a discrete set of condensed chromosomes: Ki-67–mACl localized to the external surface of chromosomes, whereas SMC2–mACh was detectable on their central axis (Fig. 4B, time 0 min). At 40 min after addition of IAA, the signals of Ki-67–mACl and SMC2–mACh started to decrease, and chromosomes tended to lose their rod-shaped morphology (Fig. 4B, time 40 min). After 60 min, both signals diminished to an undetectable level, and chromosomes form a single cluster with protrusions (Fig. 4B, time 60 min, 80 min and 100 min), whose morphology was very similar to that of the rice cake shown in Fig. 3E. In control cells in which both Ki-67 and SMC2 escaped from degradation during the imaging period, mitotic chromosomes kept their structural integrity (Fig. 4C). Taken the observations in Figs 3 and 4 together, we conclude that cells can neither establish nor maintain the structural integrity of mitotic chromosomes when both Ki-67 and SMC2 are absent.

Validation of the observed chromosome morphology by a machine learning algorithm

In the experiments above, we observed seemingly different impacts on the morphology of mitotic chromosomes caused by depletion of either Ki-67, SMC2 or both. When comparing the images of those chromosomes side by side (Fig. 5A), the defective phenotypes observed among the three cell lines were clearly distinct from each other. Nevertheless, to further validate these differences objectively and quantitatively, we used a supervised machine-learning algorithm, wndchrm (weighted neighbor distances using a compound hierarchy of algorithms representing morphology) (Ono et al., 2017; Orlov et al., 2008). We first collected 36 images of mitotic chromosomes observed under each of the four conditions (control, Ki-67 depletion, SMC2 depletion and Ki-67/ SMC2 double depletion), and each set was defined as a class. Different numbers of images (5–35 images) were randomly selected from each class, and they were subjected to wndchrm analysis for constructing classifiers. We found, as expected, that the classification accuracy (CA) obtained with those classifiers increased according to the number of images used, reaching a plateau when more than 15 images from each class were used (Fig. 5B). Then, the 36 images in each class were randomly divided into two independent subclasses (subclasses 1 and 2, each containing 18 images). The resultant eight subclasses were processed in parallel for wndchrm analysis, and the differences included in those images were statistically evaluated. The results were displayed as morphological distances (MD) between the two different subclasses (Fig. 5C) and also as a phylogeny tree (Fig. 5D). In the phylogeny tree, the two subclasses derived from each class were closely clustered with each other, confirming the validity of this classification method. Notably, the four classes were distantly branched from each other, positioning at vertices of a cruciform that had four branches of similar lengths. This result indicates that the morphology of mitotic chromosomes formed in the four different settings tested are distinct from each other, and that the defective phenotype observed in cells devoid of both Ki-67 and SMC2 is closer to neither that observed in cells devoid of Ki-67 alone nor that observed in cells devoid of SMC2 alone.

Additional characterization of the rice cake phenotype observed in cells devoid of both Ki-67 and SMC2

To further characterize the rice cake phenotype observed in cells devoid of both Ki-67 and SMC2 (Fig. 3E), those cells were fixed 1 h after the release into mitosis and subjected to immunofluorescence analyses using various antibodies (Fig. 6A–D). One of the most conspicuous observations upon depletion of both Ki-67 and SMC2 was the loss of radial arrays of microtubules and the emergence of microtubule bundles passing through the rice cake (Fig. 6A,D). Live-cell imaging performed in parallel revealed that the microtubule bundles initiated were formed at around the time of NEBD (Fig. S6A,B). These alterations of microtubule organization never happened in cells devoid of Ki-67 alone (Fig. S7A,B). In cells showing the rice cake phenotype, the centrosomes, as judged by the localization of pericentrin, were located away from the chromosome mass (Fig. 6D). Chromosomal regions containing kinetochores, as determined by the localization of Hec1 (also known as NDC80, an outer kinetochore component) and other centromere/kinetochore-associated proteins, seemed to be pulled along the microtubule bundles toward the centrosome (Fig. 6B; Fig. S7C–E), thereby producing the protrusions characteristic of the rice cake. Alternatively, it is possible that the polar ejection force powered by chromokinesins, such as Kid (also known as KIF22) and KIF4,

Journal of Cell Science (2018) 131, jcs212092. doi:10.1242/jcs.212092

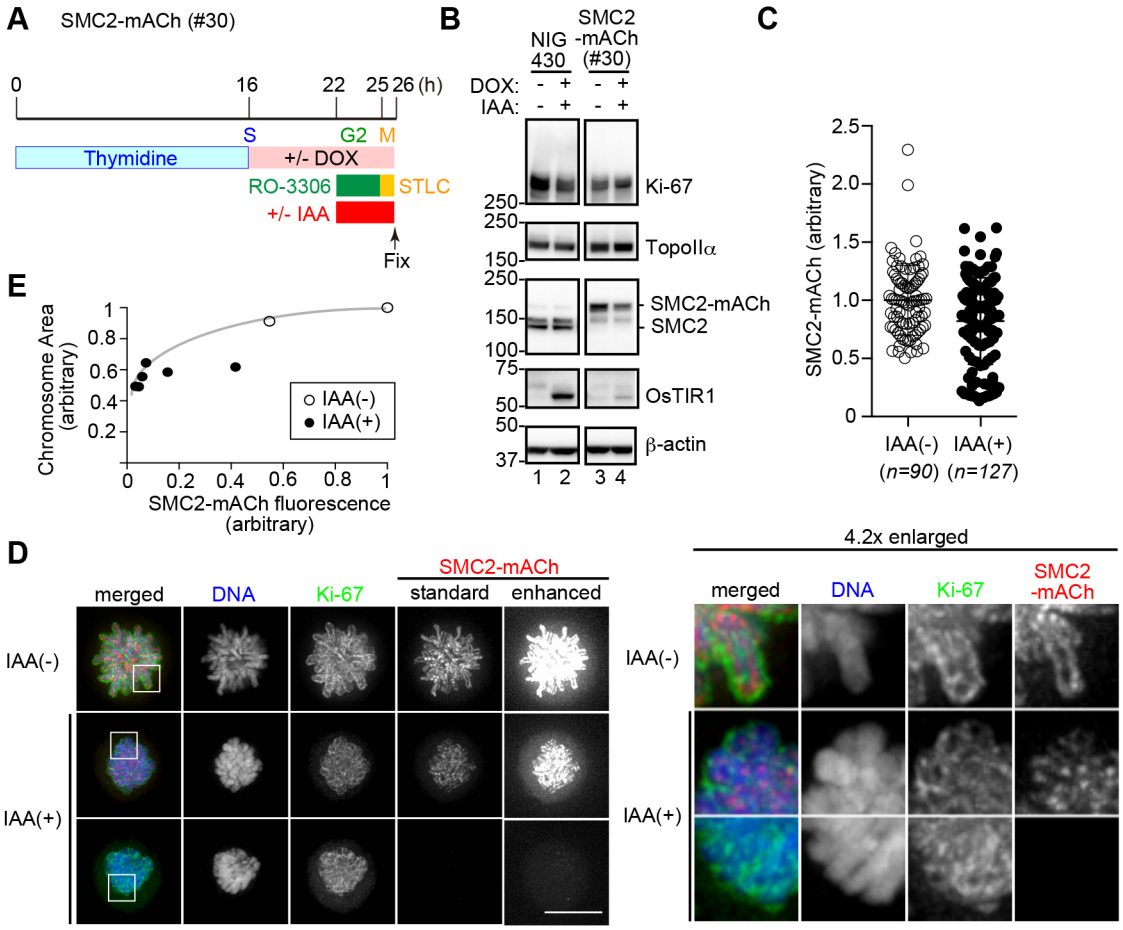

Fig. 2. Ki-67 localizes on mitotic chromosomes independently of SMC2. (A) Schematic diagram of the cell preparation protocol. Thymidine (2 mM), DOX (2 µg/ml), RO-3306 (10 µM), STLC (10 µM) and IAA (0.5 mM) were added and/or washed out at the indicated time points. AID-tagged proteins are subjected to proteasome-mediated degradation upon the treatment of cells with DOX plus IAA for 4 h. (B) Immunoblot analysis of NIG430 [a mother cell of SMC2-mACh (#30)] and SMC2-mACh (#30) cells. Membranes were probed with specific antibodies against the indicated proteins. (C) Fluorescence intensities of SMC2-mACh in SMC2-mACh (#30) cells prepared in the absence (–) or presence (+) of IAA. Each circle represents the fluorescence intensity of an individual cell relative to the average intensity of untreated SMC2-mACh (#30) cells. (D) Immunofluorescence analysis of SMC2-mACh (#30) cells prepared in the absence (–) or presence (+) of IAA. SMC2 was detected via the fluorescence of mCherry fused to the C-terminal end. Ki-67 and topo IIα were detected via indirect immunofluorescence (IF) using specific antibodies. DNA was counterstained with Hoechst 33342. Images of SMC2-mACh (#30) cells, in which SMC2–mAID–mCherry was degraded only moderately (second row) or completely (third row), are shown. The areas indicated by the white squares are 4.2-times enlarged and shown on the right. (E) Plots of chromosome areas stained with Hoechst 33342 (arbitrary units) as a function of the fluorescence intensity of SMC2–mACh in each cell. Scale bars: 10 µm.

might contribute to the formation of protrusions by pushing the whole chromosome mass in the opposite direction. Interestingly, strong signals of topo IIα were detectable along the protrusions (Fig. 6C), implying that topo IIα-enriched pericentromeric heterochromatic regions were also pulled by the microtubule bundles. In parallel with these observations, cells devoid of only SMC2 [SMC2-mACh (#30) treated with IAA] were examined (Fig. 6D, Fig. S7G–J). Although Hec1 signals were also clustered at one side of the nucleus (Fig. S7H), probably along microtubule fibers (Fig. 6D, Fig. S7G), accumulation of topo IIα on certain chromosomal regions was not clearly observed (Fig. S7I). The protrusions were less obvious in cells devoid of SMC2 alone compared to cells devoid of both Ki-67 and SMC2 (Fig. 6D; Fig. S7G–I). In fact, the distance between the centroid of chromatin mass and the Hec1-positive region was shorter in the former cells than in the latter cells (Fig. 6E). Assuming that the emergence of the Hoechst 33342-positive protrusions reflects a loss of structural integrity of chromosomes, the chromosomes devoid of both Ki-67 and SMC2 appeared more fragile than those devoid of SMC2 alone. The alteration of microtubule organization, which was accompanied with the depletion of SMC2, might contribute to and accelerate the formation of the rice-cake phenotype (see Discussion).

DISCUSSION

In the current study, we aimed to understand the functional relationship between Ki-67 and condensins in establishing and maintaining the structural integrity of mitotic chromosomes in human cells. By using a panel of HCT116-based AID cells, in which Ki-67 or subunits of condensins can be degraded conditionally, we first extended our previous finding that Ki-67 and condensins behaved independently in mitotic cells (Takagi et al., 2016). We then examined defective phenotypes caused by depletion of both Ki-67 and condensins. The defect we observed looked more severe than those obtained under any other conditions, which was further validated by the image analyses performed using the supervised machine-learning algorithm wndchrm. Our results suggest that Ki-67 and condensins have independent, yet cooperative, functions in supporting the structural integrity of mitotic chromosomes.

Journal of Cell Science (2018) 131, jcs212092. doi:10.1242/jcs.212092

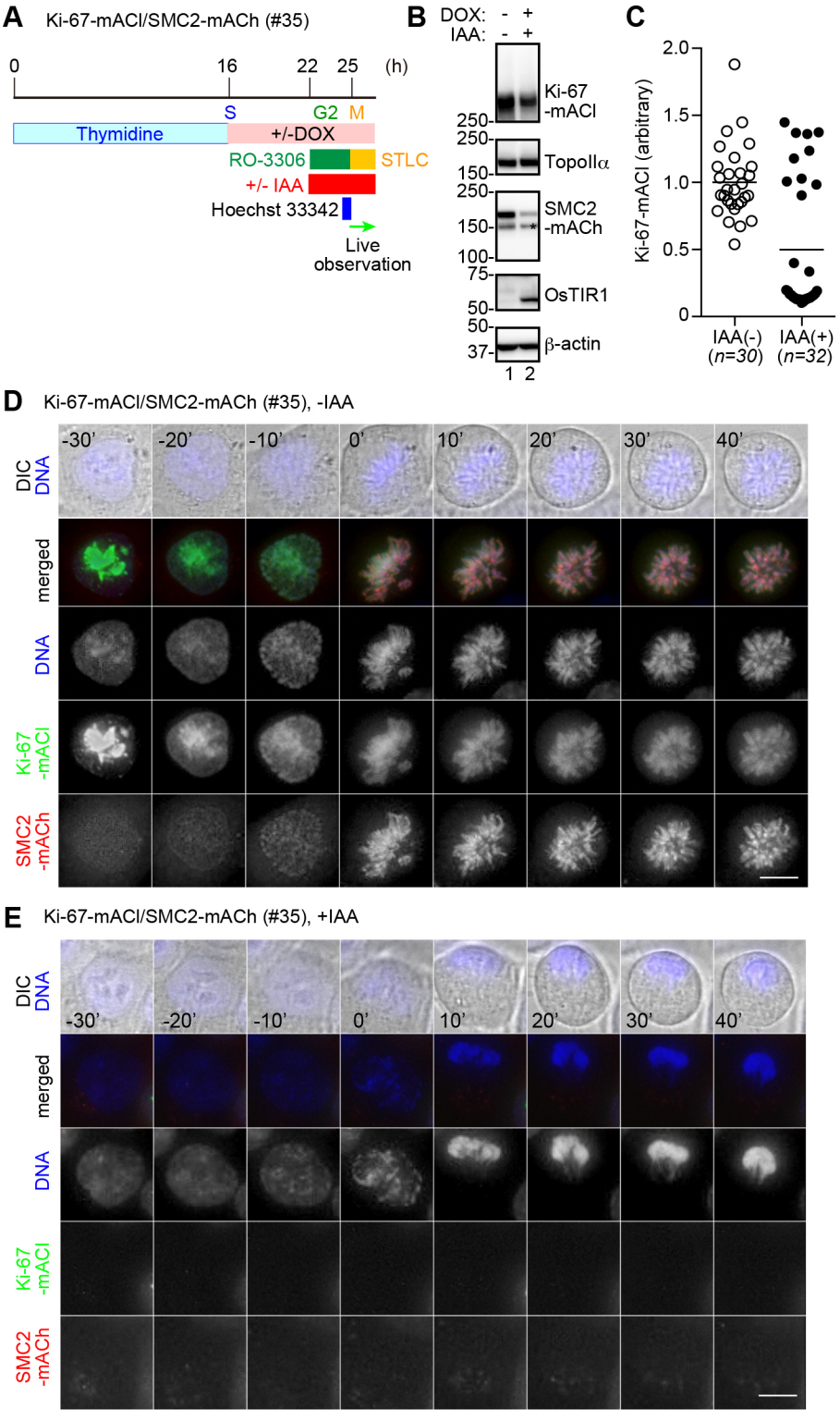

Fig. 3. Rapid loss of the structural integrity of chromosomes immediately after NEBD in cells devoid of both Ki-67 and SMC2. (A) Schematic diagram of the cell preparation protocol. Thymidine (2 mM), DOX (2 µg/ml), RO-3306 (10 µM), STLC (10 µM), Hoechst 33342 (100 ng/ml) and IAA (0.5 mM) were added and/or washed out at the indicated time points. (B) Immunoblot analysis of Ki-67-mAcI/SMC2-mACh (#35) cells. Membranes were probed with specific antibodies against the indicated proteins. (C) Fluorescence intensities of Ki-67–mAcI in Ki-67-mAcI/SMC2-mACh (#35) cells prepared in the absence (–) or presence (+) of IAA. Each circle represents the fluorescence intensity of an individual cell relative to the average intensity of untreated Ki-67-mAcI/SMC2-mACh (#35). The horizontal bars show the average intensities. (D,E) Live observation of Ki-67-mAcI/SMC2-mACh (#35) cells prepared in the absence (D) or presence (E) of IAA. Images were taken at 10-min intervals. The first frame after NEBD marks the time point 0. DIC, differential interference contrast. Shown here are representative image sets out of more than six image sets captured. Scale bars: 10 µm.

How might Ki-67 contribute to the structure of mitotic chromosomes?

In the current study, we have shown that mitotic chromosomes assembled in the absence of Ki-67 display a swollen morphology (Fig. 1C,D and 5A; Takagi et al., 2016). Consistent with this, a recent study showed that the total volume of mitotic chromosomes (DAPI-stained chromatin regions) increased by 38% upon siRNA-mediated depletion of Ki-67 in RPE-1 cells (Booth et al., 2016). Somewhat inconsistent with these data, however, is that we and others have also noticed that Ki-67 depletion has little impact on the morphology of mitotic chromosomes when they were spread on the surface of glass slides (‘mitotic spreads’) or when they were simply exposed to hypotonic buffers (Cuylen et al., 2016; data not shown). We infer that the contribution of Ki-67 to the structural integrity of mitotic chromosomes becomes apparent only when they are in close proximity in the cell, and that this situation is heavily perturbed

Journal of Cell Science (2018) 131, jcs212092. doi:10.1242/jcs.212092

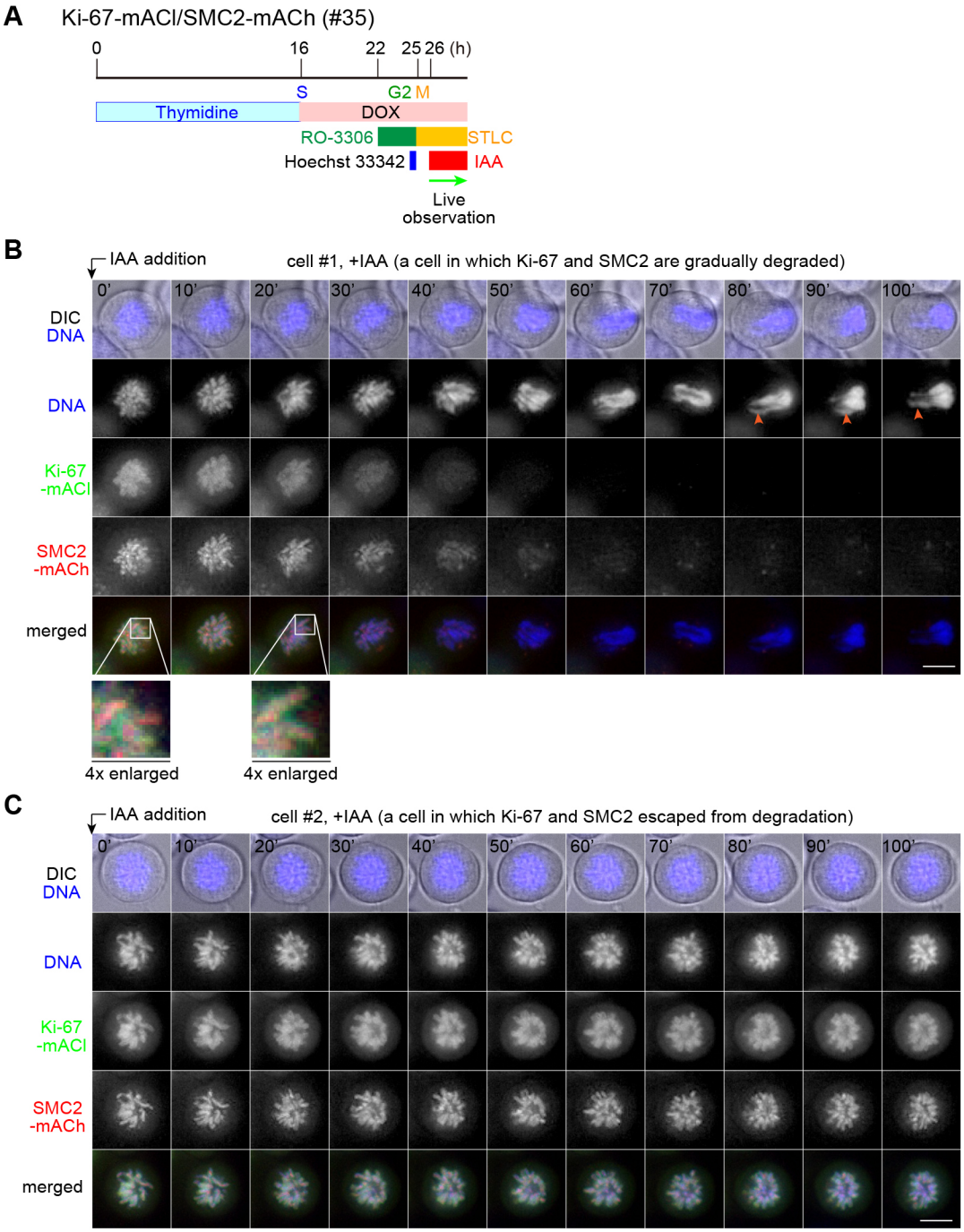

Fig. 4. Rapid loss of the structural integrity of mitotic chromosomes in cells devoid of both Ki-67 and SMC2 even after their assembly is complete. (A) Schematic diagram of the cell preparation protocol. Thymidine (2 mM), DOX (2 µg/ml), RO-3306 (10 µM), STLC (10 µM), Hoechst 33342 (100 ng/ml) and IAA (0.5 mM) were added and/or washed out at the indicated time points. AID-tagged proteins are subjected to proteasome-mediated degradation upon the treatment of cells with IAA. (B,C) Ki-67-mAcI/SMC2-mACh (#35) cells, and HCT116-based cells expressing Ki-67-mAcI and SMC2-mACh, were filmed at 10-min intervals over 100 min. In the cell #1 (B), Ki-67–mAcI and SMC2–mACh were degraded over time as expected according the protocol, and mitotic chromosomes accordingly lost their structural integrity. The characteristic protrusions are marked with arrowheads. Fourfold magnified views of selected parts of the first and third images of the cell #1 are shown in the bottom row. Cell #2 (C), in which both proteins escaped from degradation during the imaging period, is presented here as a control. DIC, differential interference contrast. Shown here are representative image sets out of more than eight image sets captured. Scale bars: 10 µm.

when the cells are exposed to hypotonic buffers and/or subjected to spreading techniques. This idea is consistent with the recent proposal that Ki-67 could function as a 'surfactant' (electrostatic charge barrier) that helps to prevent the coalescence of individual chromosomes (Cuylen et al., 2016).

Use of the AID system to acutely deplete condensins and Ki-67 from human HCT116 cells

The defective impact on chromosome appearance upon depletion of Ki-67 was seen more evidently in the experiments using the AID system (Takagi et al., 2016; this study) than in the previous

Journal of Cell Science (2018) 131, jcs212092. doi:10.1242/jcs.212092

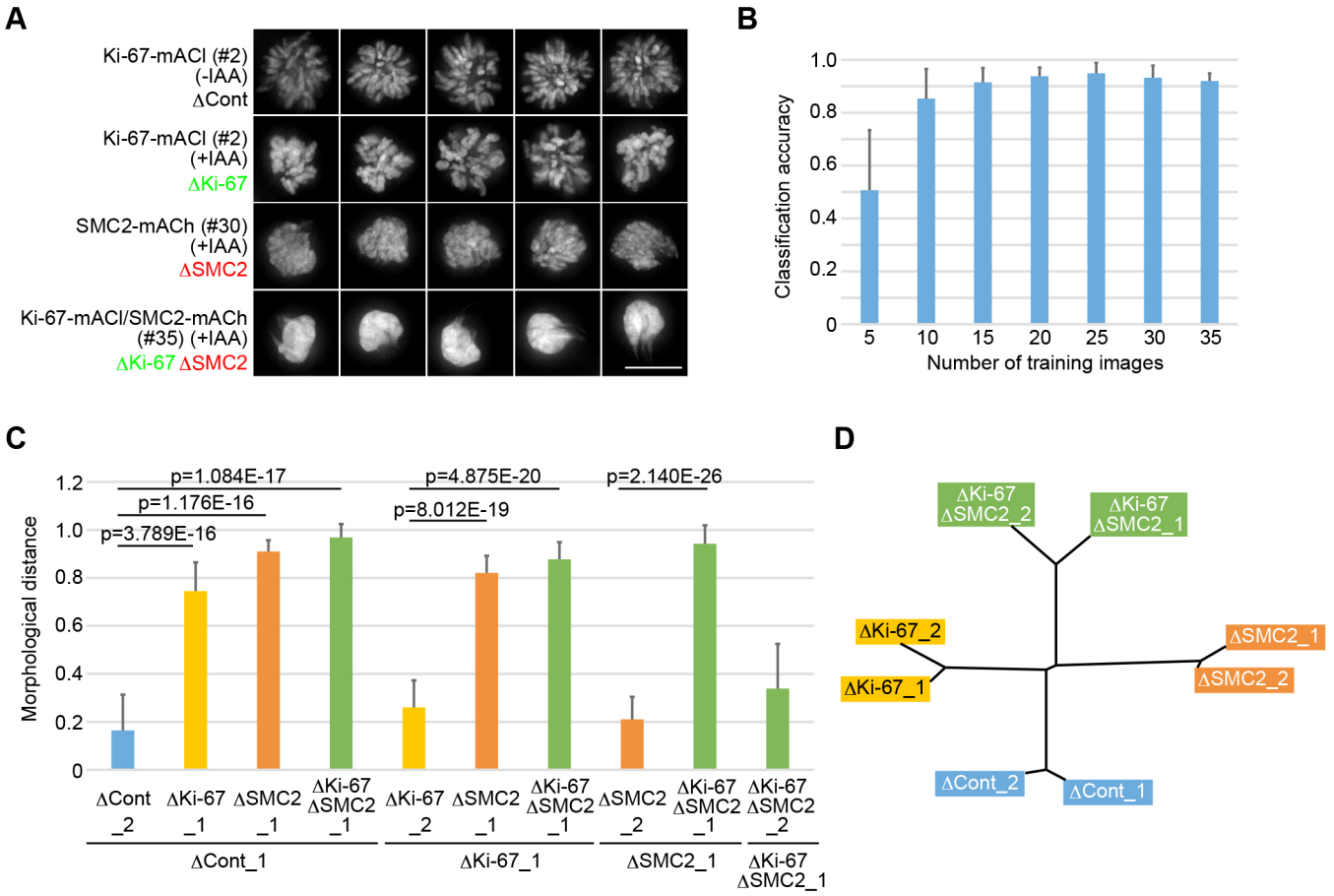

Fig. 5. Quantitative analyses of chromosome morphology as determined by using a machine-learning algorithm. (A) Representative images of mitotic chromosomes observed in four different experimental settings. The sources of the images include Ki-67-mACh (#2) cells in the absence (–) or presence (+) of IAA according to the protocol illustrated in Fig. 1A, and SMC2-mACh (#30) and Ki-67-mACl/SMC2-mACh (#35) cells in the presence (+) of IAA according to the protocol illustrated in Fig. 2A. For collecting chromosome images from the IAA-treated cells, cells were selected in which the fluorescence signals of Ki-67-mACl and/or SMC2-mACh were diminished to an undetectable level. 36 images were collected from each setting and stored as four different classes (ΔCont, ΔKi-67, ΔSMC2 and ΔKi-67ΔSMC2). Scale bar: 10 µm. (B–D) Wndchrm analysis. (B) Assessment of the optimum numbers of training images required for classification. Different numbers of images (5–35 images) from each class were used as training images for constructing classifiers. The classification accuracy (CA) of each classifier was determined by cross validation tests. The values shown are the mean±s.d. from 20 independent tests. The accuracy reached a plateau when more than 15 training images were used. (C,D) Morphological distance (MD; C) and phylogeny (D). Images obtained from each of the four settings were randomly divided into two subclasses (each containing 18 images) with one of each serving as a negative control. The MD values (C) shown are the mean±s.d. from 20 independent cross validation tests. Statistics are from a two-tailed Student's *t*-test.

experiments using siRNAs (Takagi et al., 2014; Vanneste et al., 2009). This might be explained by the quickness of Ki-67 degradation that is realized by the AID system, and also by the sure selection of cells to be observed based on the loss of fluorescence (derived from the fluorescent protein tagged tandemly to the AID). Likewise, the AID system is also a powerful system to perturb condensin functions: depletion of condensins with other methods used so far, such as siRNA transfection or transcriptional repression, has been reported to cause relatively mild defects in chromosome condensation (Gassmann et al., 2004) and in the stability of centromeres and spindle geometry (Oliveira et al., 2005; Ono et al., 2004; Samoshkin et al., 2009; Wignall et al., 2003). In the current study, we observed much clearer phenotypes in these functional aspects of condensins upon the depletion of SMC2 by using the AID system. In fact, the spindle phenotypes, such as microtubule bundling and the failure to make radial arrays in the presence of STLC, reported here (Fig. 6D, Figs S2F and S7G) were never observed in cells from which SMC2 was depleted through siRNA transfection (Fig. S2G). Consistent with this, a very recent study in which the AID system was applied to deplete SMC2 from chicken DT40 cells has reported similar spindle phenotypes (Samejima et al., 2018).

Double depletion of Ki-67 and condensins causes unprecedented severe defects in chromosome architecture and behaviors

The current study has shown that cells devoid of both Ki-67 and SMC2 fail to assemble thread-like mitotic chromosomes, instead forming a ball-like chromatin cluster with no discernible borders between individual chromosomes, which we call the 'rice cake' (Fig. 3E). This particular phenotype was different from, and much more severe, than that observed in the absence of either Ki-67 or SMC2 alone (Fig. 5A). We have also shown that the depletion of Ki-67 and SMC2 'after' the completion of chromosome assembly causes a drastic contraction of thread-like chromosomes into a chromatin cluster reminiscent of the rice cake (Fig. 4). Such a drastic phenotype has never been observed by depleting either Ki-67 (Takagi et al., 2016) or SMC2 (Fig. S2D,E) alone after the completion of chromosome assembly. Taken together with their independent behaviors in mitotic cells (Figs 1 and 2, Fig. S3), it is

Journal of Cell Science (2018) 131, jcs212092. doi:10.1242/jcs.212092

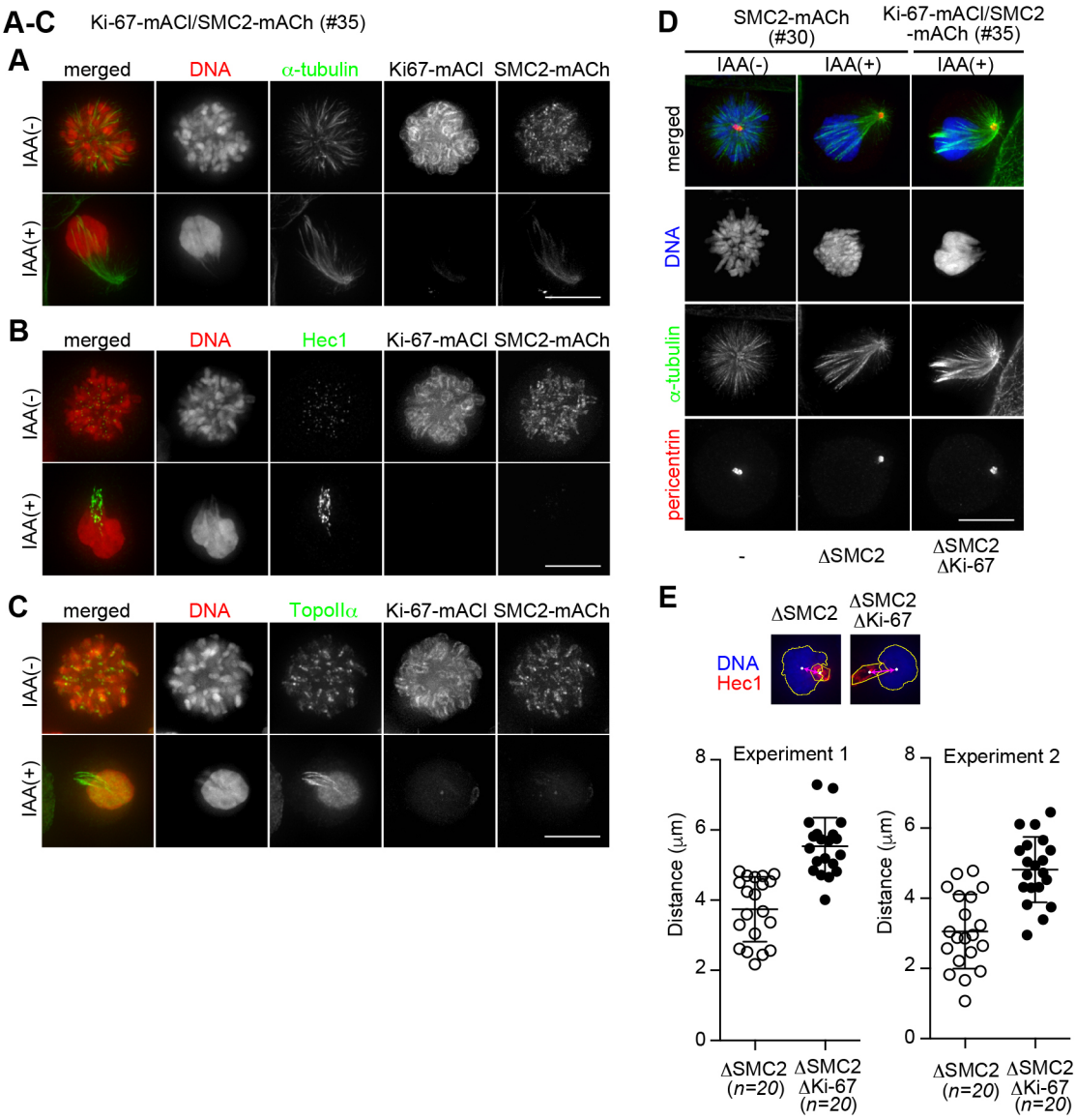

Fig. 6. Behavior of chromosomal and non-chromosomal markers in cells devoid of both Ki-67 and SMC2. Ki-67-mAcI/SMC2-mACh (#35) cells (A–C) and SMC2-mACh (#30) cells (D) were prepared in the absence (–) or presence (+) of IAA according to the protocol depicted in Fig. 2 A, and processed for immunofluorescence using antibodies against α-tubulin (A), Hec1 (B), topo IIα (C) or α-tubulin and pericentrin (D). In A–C, Ki-67 and SMC2 were detected via the fluorescence of mClover and mCherry, respectively, fused to their C-terminal ends. In D, DNA was counterstained with Hoechst 33342. Scale bars: 10 µm. (E) The distances between the centroid of the chromatin mass (blue) and the Hec1-positive region (red) of IAA-treated SMC2-mACh (#30) and Ki-67-mAcI/SMC2-mACh (#35) cells (20 cells each) were measured and plotted. The results from two independent experiments are shown, as well as the mean±s.d.

reasonable to speculate that Ki-67 and SMC2 support the structural integrity of mitotic chromosomes through distinct molecular mechanisms. What is the relationship between the two distinct mechanisms? The subunits of condensins are widely conserved among eukaryotes and play fundamental roles in the organization and segregation of mitotic chromosomes (Hirano, 2016). On the other hand, orthologs of Ki-67 are found only in vertebrates. Ki-67 could have evolved to play an auxiliary role in increasing the fidelity of segregation of chromosomes that have a large size. Such an evolutionary situation could parallel the emergence of increasing numbers of phase-separated organelles in complex organisms (Banani et al., 2017). Alternatively, non-vertebrate cells could have a peripheral chromosomal protein that plays an equivalent role to that of Ki-67 but has no sequence similarity to it.

Vertebrate cells have two different condensin complexes, condensins I and II, which behave and function differently (Green et al., 2012; Hirota et al., 2004; Ono et al., 2004). To get more insight into the mechanism behind the formation of the rice cake phenotype, we co-depleted Ki-67 with either CAP-H or CAP-H2 (Fig. S4). Double depletion of Ki-67 and CAP-H, or Ki-67 and CAP-H2 caused less-severe defects than double depletion of Ki-67 and SMC2: the chromosomes were more swollen than Ki-67-depleted chromosomes, but never produced a phenotype reminiscent of the rice cake phenotype observed in cells devoid of both Ki-67 and SMC2. Thus, loss of both functions of condensins I and II, along with loss of Ki-67, is required to create the highly characteristic defective phenotype.

Journal of Cell Science (2018) 131, jcs212092. doi:10.1242/jcs.212092

What mechanism might underlie the formation of the rice cake?

In the current study, we have shown that depletion of SMC2 alone or Ki-67 and SMC2 commonly causes microtubules to lose their radial arrays and to make bundles in STLC-treated mitotic cells (Fig. 6A,D, Fig. S7G). Microtubules still formed a radial array in STLC-treated mitotic cells even in the absence of Ki-67 (Fig. S7A). The defect in microtubule orientation is therefore specific to loss of SMC2, but not that of Ki-67. A similarly characteristic microtubule orientation was observed in STLC-treated cells when 'end-on' attachments of microtubules to kinetochores were blocked by depleting Nuf2 (Silk et al., 2009), suggesting strongly that kinetochores formed in cells devoid of SMC2 are 'laterally' attached to microtubule fibers. Consistent with the notion, α-tubulin and Hec1 showed localization patterns close to, but exclusive, from each other in cells devoid of SMC2 (Fig. S7J). It should be noted that the rice cake phenotype was observed only in cells devoid of both Ki-67 and SMC2. While the rice cake as a whole was pushed to one side in the cytoplasm to the vicinity of the cell cortex, the kinetochores were clustered at the opposite side (Fig. 6B; Fig. S7C–E) and pulled to the direction of the minus end of microtubules (Fig. 6D) probably via their lateral attachment to the bundled microtubules (Fig. S7F). Although the similar distribution of kinetochores relative to microtubule bundles occurred also in cells devoid of SMC2 alone (Fig. S7H), those kinetochores tended to stay close to the chromatin mass (Fig. 6E). We imagine that the formation of the rice cake might be based on the reduced rigidity of chromosomes, which is caused by double depletion of Ki-67 and SMC2, and accelerated by the 'unidirectional' pulling force exerted on kinetochores along the bundled microtubules, which is caused by depletion of SMC2 alone, as illustrated in Fig. S7K. In our preliminary observation using fixed cells, the rice cakes with similar morphology were observed regardless of the presence or absence of functional spindles (Fig. S6C–F). To determine unequivocally whether the pulling force exerted on kinetochores does indeed accelerate the formation of the rice cake, live-cell imaging in combination with a method that enables experimenters to label specific chromatin regions, such as one utilizing the catalytically inactive mutant of Cas9 (Chen et al., 2013; Ma et al., 2015), will be necessary and important in the future.

We verified that not only Hec1 (an outer kinetochore component; Fig. 6B) but also CENP-A (a centromeric chromatin component), CENP-I (also known as hMis6) (an inner kinetochore component) and BubR1 (a spindle check point kinase) were localized in the protrusions of the rice cake (Fig. S7C–E). These observations suggest that most, if not all, components of kinetochores remain intact within each kinetochore unit. We speculate, however, that some specific components or abilities necessary for the end-on attachments of microtubules are lost from the kinetochores in the rice cake (and similarly from those in cells devoid of SMC2 alone). It will be important to understand in the future how loss of SMC2 produces such a drastic and specific phenotype in kinetochore–microtubule attachments.

Conclusions

The key observations we made in the current study are summarized in Fig. 7. The most important finding is that cells devoid of both Ki-67 and condensins rapidly lose the structural integrity of mitotic chromosomes to an unprecedented level. In light of this finding, we propose a new concept in which Ki-67 and condensins, which localize to the external surface and the central axis of mitotic chromosomes, respectively, cooperate to support the structural integrity of mitotic chromosomes through distinct mechanisms.

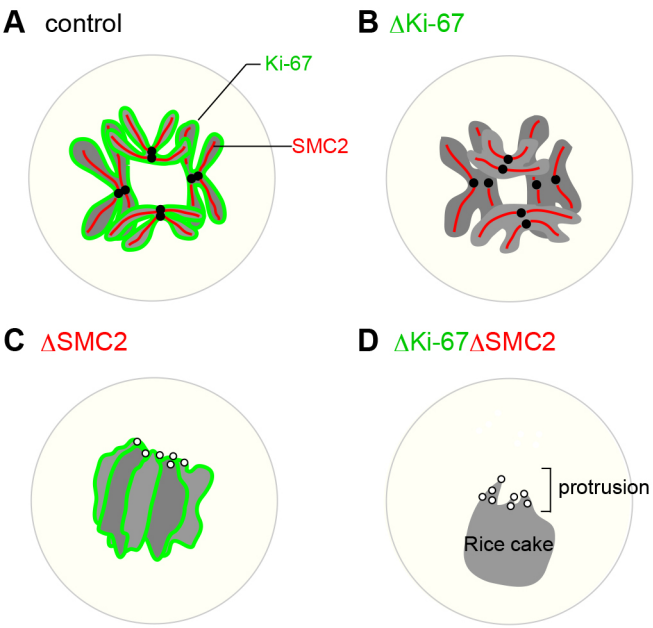

Fig. 7. Ki-67 and condensins support the integrity of mitotic chromosomes through distinct mechanisms. (A) In control cells, Ki-67 (green) and condensins (red) support the integrity of mitotic chromosomes internally and externally, respectively. (B) In cells devoid of Ki-67, mitotic chromosomes are slightly swollen and tend to coalesce with each other. (C) In cells devoid of SMC2, mitotic chromosomes are severely disorganized. The centromere or kinetochore regions tend to be clustered at the side of the chromatin mass close to the centrosome (not shown). (D) When both Ki-67 and SMC2 are depleted, all chromosomes apparently fuse to form a single cluster, which we call a 'rice cake', from which the centromere or kinetochore regions tend to protrude toward a single direction through the action of microtubules. See the text for details.

Additionally, we suggest that the contacts and interferences among mitotic chromosomes must be restricted through the action of Ki-67, otherwise the chromosome morphology would be adversely affected.

MATERIALS AND METHODS

Establishment of cell lines and their handling

HCT116 cells and its derivatives were cultured at 37°C with 5% CO_2 in DMEM supplemented with 10% fetal bovine serum (FBS). A panel of cells were generated from HCT116 cells via successive uses of CRISPR/Cas9-mediated genome editing as described previously (Natsume et al., 2016). Briefly, as the first step, the constitutive or DOX-inducible expression units of *Os*TIR1 was integrated in the AAVS1 locus of the HCT116 genome to generate cells called NIG272 or NIG430, respectively (Natsume et al., 2016). In these cells, as the second step, cassette sequences encoding variable tags were knocked-in immediately upstream of the stop codons of genes to be analyzed. Table S1 contains a list of the parental lines, the target genes, the type of tag, the sequences of guide RNAs, the plasmid names for the targeting and knock-in constructs, and antibiotics used for generating AID cells. Of cellular clones selected by their resistance to antibiotics (700 µg/ml neomycin or 100 µg/ml hygromycin B), the final selection of Ki-67-mACl/CAP-H-Ch (#11) and Ki-67-mACl/CAP-H2-Ch (#44) were carried out visually by performing fluorescence microscopy. For other cell lines, clones in which the genome had been edited as designed in both alleles were selected by means of genomic PCRs using KOD-plus-Neo (TOYOBO, Osaka, Japan) and appropriate primer sets, as listed in Table S2. Successful editing in both alleles was further confirmed by immunoblotting (to check the loss of target proteins of their original size). Cells used in this study were not recently authenticated nor tested for contamination.

Journal of Cell Science (2018) 131, jcs212092. doi:10.1242/jcs.212092

For fixed-cell immunofluorescence, cells were seeded on coverslips treated with 10 µg/ml fibronectin (Wako, Osaka, Japan). For live-cell imaging, including FRAP analysis, cells were seeded onto glass-bottom dishes (IWAKI, Tokyo, Japan). 2×10^5 cells were plated on a 35-mm dish (either a glass-bottom dish or a polystyrene dish containing four fibronectin-coated round coverslips) 1 day before the experiments and processed as follows. Cells were treated with 2 mM thymidine for 16 h, released in thymidine-free medium for 6–8 h, treated with 10 µM RO-3306 (Tocris, Minneapolis, MN) for 3 h, to cause an arrest at the G2/M boundary, and then released in medium containing 10 µM STLC (Tokyo Chemical Industry, Tokyo, Japan) to cause arrest in mitosis. In some experiments shown in Fig. S6E,F, 100 ng/ml nocodazole or 10 µM taxol (Paclitaxel; Sigma-Aldrich, St Louis, MO) was used instead of STLC. Cells were mock-treated or treated with 0.5 mM IAA (Tokyo Chemical Industry) during the period depicted in Figs 1A, 2A, 3A and 4A, Figs S1D, S2A,D, S5A, S6A,C. For the observations of AID cells derived from NIG430 [SMC2-mACh (#30) and Ki-67-mACl/SMC2-mACh (#35)], incubation with 2 µg/ml DOX (MP Biomedicals, Santa Ana, CA) after the release from thymidine block was included to induce the expression of *Os*TIR1. For probing DNA in live-cell observations, cells were treated with 100 ng/ml Hoechst 33342 30 min before removing RO-3306. For the experiment shown in Fig. S6A,B, cells were transfected with a construct encoding GFP–α-tubulin using FuGene HD (Promega, Fitchburg, WI) 4 h before initiating the synchronization procedure.

Immunoblotting

Cells were washed twice with ice-cold PBS supplemented with 0.3 mM PMSF, collected by centrifugation, and snap-frozen in liquid nitrogen. Cell pellets were resuspended in buffer B [20 mM Tris-HCl pH 7.5, 150 mM NaCl, 5 mM $MgCl_2$, 0.1% NP-40, 1 mM DTT, Complete protease inhibitor Mixture (Roche, Basel, Switzerland), and PhosSTOP (Roche)] supplemented with 0.25 units/ml Benzonase (Novagen, Madison, WI), kept on ice for 30 min, mixed with the same volume of 4× concentrated sample buffer (250 mM Tris-HCl pH 6.8, 8% SDS, 40% glycerol, 0.02% Bromophenol Blue and 0.1 M DTT), and heated at 95°C. The denatured protein samples were electrophoretically separated on a SuperSep Ace 5–20% gradient gel (Wako, Osaka, Japan) and blotted onto an Immobilon-P membrane (Merck Millipore, Billerica, MA). The following antibodies were used as primary antibodies at the indicated dilutions or concentrations: mouse anti-β-actin (1:5000, AC-15; Sigma-Aldrich, St Louis, MO), rabbit anti-NCAPH/CAP-H (1:1000, 11515-1; ProteinTech, Rosemont, IL), rabbit anti-CAP-H2 (1 µg/ml, AfR205-4L; Ono et al., 2003), rabbit anti-Ki-67 (1:1000, sc-15402; Santa Cruz Biotechnology, Dallas, TX), rabbit-*Os*TIR1 (1:1000; Natsume et al., 2016), rabbit anti-SMC2 (1:1000, ab10412; Abcam, Cambridge, UK), and mouse anti-topoisomerase IIα (1:2000, 1C5; MBL, Nagoya, Japan) antibodies. The following antibodies were used as secondary antibodies at the indicated dilutions: goat anti-mouse-IgG conjugated to horseradish peroxidase (HRP) (1:3000, 170-6516; Bio-Rad, Hercules, CA), and goat anti-rabbit-IgG conjugated to HRP (1:3000, 170-6515; Bio-Rad) antibodies. Protein bands were visualized by chemiluminescence using Immobilon Western (Merck Millipore).

Immunofluorescence

At 1 h after the removal of RO-3306, cells were fixed with 3.7% paraformaldehyde (PFA) in PBS at room temperature for 10 min. The fixed cells were permeabilized with 0.5% Triton X-100 in PBS for 5 min, blocked with a blocking solution (PBS containing 5 mg/ml BSA and 50 mM glycine) for 1 h, and processed for immunofluorescence. The following antibodies were used as primary antibodies at the indicated dilutions: mouse anti-α-tubulin (1:10,000, DM1A; Sigma-Aldrich), mouse anti-BubR1 (1:400, 8G1; MBL), mouse anti-CENP-A (1:200, 3-19; MBL), rat anti-CENP-I/hMis6 (1:100, PD032; MBL), mouse anti-HEC1 (1:1000, 9G3; GeneTex, Irvine, CA), rabbit anti-Ki-67 (1:200, sc-15402; Santa Cruz Biotechnology), mouse anti-Ki-67 (1:500, NA-59; Merck Millipore), rabbit anti-pericentrin (1:1000, ab4448; Abcam) and mouse anti-topoisomerase IIα (1:1000, 1C5; MBL) antibodies. Secondary antibodies conjugated to Alexa Fluor 488, 594 or 647 were purchased from Thermo Fisher Science (Waltham, MA). DNA was counterstained with 0.5 µg/ml Hoechst 33342. Immunofluorescence images were captured with a DeltaVision Core system (Applied Precision, Issaquah, WA) with an inverted microscope (IX71; Olympus, Tokyo, Japan), an UPlanApo 60×1.40 NA objective lens (Olympus), and a CoolSNAP HQ2 camera (Photometrics, Tucson, AZ). Images from *z* sections spaced 0.5 µm apart were acquired, deconvolved with softWorx (Applied Precision), and presented as maximum intensity projections.

Quantification of fluorescence intensities

Cells were fixed and stained with Hoechst 33342 as described above. Images of chromatin stained with Hoechst 33342 and the fluorescent proteins to be quantified were captured and processed as described above except for the use of an UPlanFL 40×0.75 NA objective lens (Olympus). Chromosomal regions were determined based on the Hoechst 33342-stained images, and the total pixel intensities of fluorescence images from those regions were calculated. The obtained values were normalized to those in the average value of control cells (cells not treated with IAA) and plotted using GraphPad Prism6 (GraphPad Software, La Jolla, CA).

FRAP

For FRAP experiments, we first attempted to generate a cell line expressing Ki-67–mClover plus SMC2–mACh, but without success. We therefore decided to use Ki-67-mACl/CAP-H-mACh (#14) (a cell line expressing Ki-67–mACl plus CAP-H–mACh) which had been generated for other purposes (Fig. S4). Note that SMC2 is not tagged with mAID in Ki-67-mACl/CAP-H-mACh (#14) cells. FRAP experiments were performed with a laser scanning confocal microscope FV1200 (Olympus) equipped with PLAPON 60 × 1.42 NA lens (Olympus). Cells expressing Ki-67–mACl and CAP-H–mACh from their intrinsic promotors [Ki-67-mACl/CAP-H-mACh (#14)] were transfected with siControl (5′-CGUACGCGGAAUACUUC-GAdTdT-3′; Elbashir et al., 2001) or siSMC2 (5′-UGCUAUCACUGGC-UUAAUdTdT-3′; Gerlich et al., 2006) at 0 and 24 h at a final concentration of 10 nM using Lipofectamine RNAiMAX (Thermo Fisher Scientific), and synchronized in mitosis as described above. The cells were transferred to a humidified environmental chamber (Stage Top Incubator; TOKAI HIT, Shizuoka, Japan) maintaining its temperature at 37°C and the CO_2 concentration at 5%, and subjected to FRAP analysis within 100 min after the release from the cell cycle arrest with RO-3306. One pre-bleach frame followed by 2 s bleach time with a 473 nm laser line at 80% transmission, and 8-10 post-bleach frames were recorded at 30 s intervals. In parallel with the signal of Ki-67-mACl, the signals of CAP-H-mACh and DNA (stained with Hoechst 33342) were recorded. The mean mClover fluorescence intensities of the bleached chromatin region for each time point was normalized to that of unbleached chromatin region at the same time point within the same cell. As cells tended to move slightly during the imaging time, the measurement areas were corrected manually relying on the chromatin images. The value for each time point was further normalized to that at the pre-bleached frame.

Live-cell observations

Cells cultured in a glass-bottom dish were mounted on an inverted microscope (IX71, Olympus) equipped with a humidified environment chamber (MI-IBC, Olympus) to maintain its temperature at 37°C and the CO_2 concentration at 5%. Fluorescence images were collected with a DeltaVision Core (Applied Precision) from *z* sections (five sections spanning 8 µm for Fig. 3, Fig. S2B,C,E, S5 and S6B; five sections spanning 2 µm for Fig. 4) every 2 min (Figs S5 and S6B) or 10 min (Figs 3 and 4, Fig. S2B,C,E) with 2×2 binning and are presented as maximum intensity projections. Differential interference microscope images were acquired in parallel from a single focal plane.

Morphological quantification of chromosome with wndchrm

Microscopic images of chromosomes were obtained from fixed cells stained with Hoechst 33342 using DeltaVision Core (Applied Precision) with an UPlanApo 60×1.40 NA objective lens (Olympus). Images from *z* sections (24 sections spanning 11.5 µm) were obtained, deconvolved and presented as maximum intensity projections. For quantitative assessment of chromosome structures, a supervised machine-learning algorithm, wndchrm (weight neighbor distance using a computed hierarchy of algorithms representing

morphology) ver. 1.52 (Ono et al., 2017; Orlov et al., 2008; Tokunaga et al., 2014), was applied to 36 projected images (188×188 pixels, 8 bit) in each condition, which was defined as a class. All of the images in the defined class were applied to wndchrm, and morphological feature values were assigned by training a machine. Phylogenies were computed by using the Fitch–Margoliash method implemented in the PHYLIP package ver. 3.696, which was based on pairwise class similarity values reported by wndchrm ver. 1.52 (Felsensein, 1989; Johnston et al., 2008). For each analysis, cross-validation tests were automatically repeated 20 times with 13 training images for each 5 image test image data set. The options used for the image analysis were a large feature set of 2919 (−l) and multi- processors (−m). To measure pairwise class dissimilarity, morphological distances (MD) were calculated as the Euclidean distances [$d=\sqrt{\sum(A-B)^2}$] from the values in class probability matrix obtained from the cross validations (Johnston et al., 2008). To calculate *P* values, two-sided Student's *t*-tests were performed for each of the comparisons. To optimize the classification capacity, we measured classification accuracy (CA) by using different numbers of training data sets, and found that the accuracy reached a plateau with more than 15 images (Fig. 5B). Then, each image in a class (36 images) was randomly assigned to one of two independent sets (folder 1 and folder 2, each containing 18 images) to confirm that images within the same class (condition) show negligible differences. They were expected to localize closely in phylogenies and to show low MD between them.

Measurement of the distance between chromatin mass and Hec1-distributed region

Microscopy images of chromosomes and Hec1 staining were obtained using the DeltaVision Core system (Applied Precision) with an UPlanApo 60×1.40 NA objective lens (Olympus). Images from *z* sections (40 sections spanning 7.8 µm) were obtained, deconvolved and presented as maximum intensity projections under the same conditions. Chromosomal regions were determined by thresholding the chromosomal images. To delineate Hec1-positive regions, the 'convex hull' of Hec1 signals was determined manually from the uniformly binarized images of Hec1. The distances between the centroids of these two regions were measured and plotted using GraphPad Prism6 (GrapPad Software).

Acknowledgements

We thank RIKEN BSI-Olympus Collaboration Center for the technical assistance with the FRAP experiment.

Competing interests

The authors declare no competing or financial interests.

Author contributions

Conceptualization: M.T., T.H.; Methodology: T.O., T.N., M.N., N.S., M.T.K.; Investigation: M.T., C.S., N.S.; Resources: T.N., M.T.K.; Writing - original draft: M.T.; Writing - review & editing: T.H.; Supervision: N.I.; Funding acquisition: M.T., T.O., T.N., M.N., N.S., M.T.K., T.H., N.I.

Funding

This work was supported by the Japan Society for the Promotion of Science (JSPS) KAKENHI (26650070 and 17K07399 to M.T., 16K07455 to T.O., 15K18482 and 17K15068 to T.N., 16K15095 to M.T.K., 25116009 and 16H04744 to N.S., 15H04707 to M.N., 26251003 to T.H., 15H05929 to N.I.). M.T.K. was supported by a grant from the Mochida Memorial Foundation for Medical and Pharmaceutical Research, the SGH Foundation, the Sumitomo Foundation and the Canon Foundation for Scientific Research.

Supplementary information

Supplementary information available online at
http://jcs.biologists.org/lookup/doi/10.1242/jcs.212092.supplemental

References

Banani, S. F., Lee, H. O., Hyman, A. A. and Rosen, M. K. (2017). Biomolecular condensates: organizers of cellular biochemistry. *Nat. Rev. Mol. Cell Biol.* **18**, 285-298.

Booth, D. G., Takagi, M., Sanchez-Pulido, L., Petfalski, E., Vargiu, G., Samejima, K., Imamoto, N., Ponting, C. P., Tollervey, D., Earnshaw, W. C. et al. (2014). Ki-67 is a PP1-interacting protein that organises the mitotic chromosome periphery. *Elife* **3**, e01641.

Booth, D. G., Beckett, A. J., Molina, O., Samejima, I., Masumoto, H., Kouprina, N., Larionov, V., Prior, I. A. and Earnshaw, W. C. (2016). 3D-CLEM reveals that a major portion of mitotic chromosomes is not chromatin. *Mol. Cell* **64**, 790-802.

Chen, B., Gilbert, L. A., Cimini, B. A., Schnitzbauer, J., Zhang, W., Li, G.-W., Park, J., Blackburn, E. H., Weissman, J. S., Qi, L. S. et al. (2013). Dynamic imaging of genomic loci in living human cells by an optimized CRISPR/Cas system. *Cell* **155**, 1479-1491.

Cuylen, S., Blaukopf, C., Politi, A. Z., Müller-Reichert, T., Neumann, B., Poser, I., Ellenberg, J., Hyman, A. A. and Gerlich, D. W. (2016). Ki-67 acts as a biological surfactant to disperse mitotic chromosomes. *Nature* **535**, 308-312.

Elbashir, S. M., Harborth, J., Lendeckel, W., Yalcin, A., Weber, K. and Tuschl, T. (2001). Duplexes of 21-nucleotide RNAs mediated RNA interference in cultured mammalian cells. *Nature* **411**, 494-498.

Felsensein J. (1989). PHYLIP: phylogeny inference package (version 3.2). Cladistics **5**, 164-166.

Gassmann, R., Vagnarelli, P., Hudson, D. and Earnshaw, W. C. (2004). Mitotic chromosome formation and the condensin paradox. *Exp. Cell Res.* **296**, 35-42.

Gerlich, D., Hirota, T., Koch, B., Peters, J.-M. and Ellenberg, J. (2006). Condensin I stabilizes chromosomes mechanically through a dynamic interaction in live cells. *Curr. Biol.* **16**, 333-344.

Green, L. C., Kalitsis, P., Chang, T. M., Cipetic, M., Kim, J. H., Marshall, O., Turnbull, L., Whitchurch, C. B., Vagnarelli, P., Samejima, K. et al. (2012). Contrasting roles of condensin I and condensin II in mitotic chromosome formation. *J. Cell Sci.* **125**, 1591-1604.

Hirano, T. (2016). Condensin-based chromosome organization from bacteria to vertebrates. *Cell* **164**, 847-857.

Hirota, T., Gerlich, D., Koch, B., Ellenberg, J. and Peters, J. M. (2004). Distinct functions of condensin I and II in mitotic chromosome assembly. *J. Cell Sci.* **117**, 6435-6445.

Johnston, J., Iser, W. B., Chow, D. K., Goldberg, I. G. and Wolkow, C. A. (2008). Quantitative image analysis reveals distinct structural transitions during aging in Caenorhabditis elegans tissues. *PLoS ONE* **3**, e2821.

Ma, H., Naseri, A., Reyes-Gutierrez, P., Wolfe, S. A., Zhang, S. and Pederson, T. (2015). Multicolor CRISPR labeling of chromosomal loci in human cells. *Proc. Natl. Acad. Sci. USA* **112**, 3002-3007.

Maresca, T. J., Freedman, B. S. and Heald, R. (2005). Histone H1 is essential for mitotic chromosome architecture and segregation in Xenopus laevis egg extracts. *J. Cell Biol.* **169**, 859-869.

Mazumdar, M., Lee, J.-H., Sengupta, K., Ried, T., Rane, S. and Misteli, T. (2006). Tumor formation via loss of a molecular motor protein. *Curr. Biol.* **16**, 1559-1564.

Natsume, T., Kiyomitsu, T., Saga, Y. and Kanemaki, M. T. (2016). Rapid protein depletion in human cells by auxin-inducible degron tagging with short homology donors. *Cell Rep.* **15**, 210-218.

Oliveira, R. A., Coelho, P. A. and Sunkel, C. E. (2005). The condensin I subunit Barren/CAP-H is essential for the structural integrity of centromeric heterochromatin during mitosis. *Mol. Cell. Biol.* **25**, 8971-8984.

Ono, T., Fang, Y., Spector, D. L. and Hirano, T. (2004). Spatial and temporal regulation of Condensins I and II in mitotic chromosome assembly in human cells. *Mol. Biol. Cell* **15**, 3296-3308.

Ono, T., Losada, A., Hirano, M., Myers, M. P., Neuwald, A. F. and Hirano, T. (2003). Differential contributions of condensin I and condensin II to mitotic chromosome architecture in vertebrate cells. *Cell* **115**, 109-121.

Ono, T., Sakamoto, C., Nakao, M., Saitoh, N. and Hirano, T. (2017). Condensin II plays an essential role in reversible assembly of mitotic chromosomes in situ. *Mol. Biol. Cell* **28**, 2375-2886.

Orlov, N., Shamir, L., Macura, T., Johnston, J., Eckley, D. M. and Goldberg, I. G. (2008). WND-CHARM: Multi-purpose image classification using compound image transforms. *Pattern Recognit. Lett.* **29**, 1684-1693.

Saiwaki, T., Kotera, I., Sasaki, M., Takagi, M. and Yoneda, Y. (2005). In vivo dynamics and kinetics of pKi-67: transition from a mobile to an immobile form at the onset of anaphase. *Exp. Cell Res.* **308**, 123-134.

Samejima, K., Samejima, I., Vagnarelli, P., Ogawa, H., Vargiu, G., Kelly, D. A., de Lima Alves, F., Kerr, A., Green, L. C., Hudson, D. F. et al. (2012). Mitotic chromosomes are compacted laterally by KIF4 and condensin and axially by topoisomerase IIalpha. *J. Cell Biol.* **199**, 755-770.

Samejima, K., Booth, D. G., Ogawa, H., Paulson, J. R., Xie, L., Watson, C. A., Platani, M., Kanemaki, M. T. and Earnshaw, W. C. (2018). Rapid degradation of condensins and 3D-EM reveal chromatin volume is uncoupled from chromosome architecture in mitosis. *J. Cell Sci.* **131**, jcs210187.

Samoshkin, A., Arnaoutov, A., Jansen, L. E. T., Ouspenski, I., Dye, L., Karpova, T., McNally, J., Dasso, M., Cleveland, D. W. and Strunnikov, A. (2009). Human condensin function is essential for centromeric chromatin assembly and proper sister kinetochore orientation. *PLoS ONE* **4**, e6831.

Scholzen, T. and Gerdes, J. (2000). The Ki-67 protein: from the known and the unknown. *J. Cell. Physiol.* **182**, 311-322.

Shintomi, K., Takahashi, T. S. and Hirano, T. (2015). Reconstitution of mitotic chromatids with a minimum set of purified factors. *Nat. Cell Biol.* **17**, 1014-1023.

Silk, A. D., Holland, A. J. and Cleveland, D. W. (2009). Requirements for NuMA in maintenance and establishment of mammalian spindle poles. *J. Cell Biol.* **184**, 677-690.

Takagi, M., Nishiyama, Y., Taguchi, A. and Imamoto, N. (2014). Ki67 antigen contributes to the timely accumulation of protein phosphatase 1gamma on anaphase chromosomes. *J. Biol. Chem.* **289**, 22877-22887.

Takagi, M., Natsume, T., Kanemaki, M. T. and Imamoto, N. (2016). Perichromosomal protein Ki67 supports mitotic chromosome architecture. *Genes Cells* **21**, 1113-1124.

Takahashi, M., Wakai, T. and Hirota, T. (2016). Condensin I-mediated mitotic chromosome assembly requires association with chromokinesin KIF4A. *Genes Dev.* **30**, 1931-1936.

Tokunaga, K., Saitoh, N., Goldberg, I. G., Sakamoto, C., Yasuda, Y., Yoshida, Y., Yamanaka, S. and Nakao, M. (2014). Computational image analysis of colony and nuclear morphology to evaluate human induced pluripotent stem cells. *Sci. Rep.* **4**, 6996.

Uhlmann, F. (2016). SMC complexes: from DNA to chromosomes. *Nat. Rev. Mol. Cell Biol.* **17**, 399-412.

Vanneste, D., Takagi, M., Imamoto, N. and Vernos, I. (2009). The role of Hklp2 in the stabilization and maintenance of spindle bipolarity. *Curr. Biol.* **19**, 1712-1717.

Wignall, S. M., Deehan, R., Maresca, T. J. and Heald, R. (2003). The condensin complex is required for proper spindle assembly and chromosome segregation in Xenopus egg extracts. *J. Cell Biol.* **161**, 1041-1051.